tvst

Retina

A Pixel-Based Machine-Learning Model For Three-Dimensional Reconstruction of Vitreous Anatomy

Alan Thi[1], K. Bailey Freund[1,2], and Michael Engelbert[1,2]

[1] Vitreous Retina Macula Consultants of New York, New York, NY, USA
[2] NYU Grossman School of Medicine, Department of Ophthalmology, New York, NY, USA

Correspondence: Michael Engelbert, Vitreous Retina Macula Consultants of New York, 460 Park Ave. New York, NY 10022, USA. e-mail: michael.engelbert@gmail.com

Received: January 24, 2022
Accepted: June 4, 2022
Published: July 8, 2022

Keywords: vitreous; imaging; OCT; machine learning; anatomy

Citation: Thi A, Freund KB, Engelbert M. A pixel-based machine-learning model for three-dimensional reconstruction of vitreous anatomy. Transl Vis Sci Technol. 2022;11(7):3, https://doi.org/10.1167/tvst.11.7.3

Purpose: To develop a machine-learning image processing model for three-dimensional (3D) reconstruction of vitreous anatomy visualized with swept-source optical coherence tomography (SS-OCT).

Methods: Healthy subjects were imaged with SS-OCT. Scans of sufficient quality were transferred into the Fiji is just ImageJ image processing toolkit, and proportions of the resulting stacks were adjusted to form cubic voxels. Image-averaging and Trainable Weka Segmentation using Sobel and variance edge detection and directional membrane projections filters were used to enhance and interpret the signals from vitreous gel, liquid spaces within the vitreous, and interfaces between the former. Two classes were defined: "Septa" and "Other." Pixels were selected and added to each class to train the classifier. Results were generated as a probability map. Thresholding was performed to remove pixels that were classified with low confidence. Volume rendering was performed with TomViz.

Results: Forty-seven eyes of 34 healthy subjects were imaged with SS-OCT. Thirty-four cube scans from 25 subjects were of sufficient quality for volume rendering. Clinically relevant vitreous features including the premacular bursa, area of Martegiani, and prevascular vitreous fissures and cisterns, as well as varying degrees of vitreous degeneration were visualized in 3D.

Conclusions: A machine-learning model for 3D vitreous reconstruction of SS-OCT cube scans was developed. The resultant high-resolution 3D movies illustrated vitreous anatomy in a manner like triamcinolone-assisted vitrectomy or postmortem dye injection.

Translational Relevance: This machine learning model now allows for comprehensive examination of the vitreous structure beyond the vitreoretinal interface in 3D with potential applications for common disease states such as the vitreomacular traction and Macular Hole spectrum of diseases or proliferative diabetic retinopathy.

Introduction

The anatomy of the vitreous is notoriously difficult to visualize in vivo and postmortem. Worst,[1,2] Kishi and Shimizu,[3] Eisner,[4,5] and Sebag[6] have visualized the vitreous body in three dimensions (3D) by carefully preparing cadaver eyes and often staining or injecting them with dye. In addition to the prepapillary gap[4,5] in the area of Martegiani, these methods revealed various liquid vitreous spaces, such as the premacular bursa[1,2] or posterior precortical vitreous pocket,[3] and prevascular vitreous fissures[4,5] and cisterns,[1,2] which had not been previously detected. This was probably due in large part to their high optical transmittance. Although these methods produced valuable information, they did not allow for examining the vitreous in vivo. Furthermore, these delicate structures are prone to damage during handling and preparation, as well as postmortem decomposition. All these factors add potential confounding factors and limit the ability to correlate anatomy with pathology.

Previous studies have shown that swept-source optical coherence tomography (SS-OCT) produces

superior images of the vitreous structures compared to spectral-domain OCT.[7,8] By moving choroid and retina OCT signals toward the bottom of the acquisition window and prioritizing the vitreous, an operator of a Zeiss Plex-Elite 9000 SS-OCT (Carl Zeiss Meditec, Inc, Dublin, CA, USA) is able to capture 12 × 12 mm cube scans that include the posterior portion of the vitreous body.[9] Despite these techniques, the signal-to-noise ratio in the vitreous is low, and although the liquid spaces within the vitreous and other features of its anatomy are recognizable on OCT-scans, conventional 3D reconstruction does not yield images that represent the gel and liquid spaces of the vitreous that are similar to what can routinely be seen during triamcinolone-aided vitrectomy.

Image segmentation, the process of partitioning digital images into non-intersecting regions, are traditionally based on the intensity information of pixels.[10] However, the clinician uses much more knowledge when interpreting an image. In recent years, trainable image processing algorithms have been developed to include some of this knowledge in the segmentation process.

In this study, we used the Waikato Environment for Knowledge Analysis (WEKA) FastRandomForest classifier implemented in the Trainable Weka Segmentation[11] plugin, an interactive trainable segmentation algorithm, to identify the liquid spaces and their boundaries within the posterior vitreous cavity and reconstruct them in 3D.

Methods

Study Subjects

Our study adhered to the tenets of the Declaration of Helsinki on the ethical principles of medical research and complied with the Health Insurance Portability and Accountability Act of 1996. It was approved by the Western Institutional Review Board committee. Written informed consent was obtained from each participant.

Healthy participants with attached vitreous and no known anterior segment or vitreoretinal pathology were enrolled prospectively in this study.

Image Acquisition

All eyes were imaged on the PLEX Elite 9000 (Carl Zeiss Meditec, Inc) OCT device. The PLEX Elite 9000 uses a swept-source laser with a center wavelength of 1040 to 1060 nm and a scan speed of 100,000 A-scans per second. Cube (12 × 12 mm) scans comprising 1024 B-scans (each comprising 1024 A-scans) with a scan depth of 6 mm centered at the fovea were obtained for each pharmacologically dilated study eye (phenylephrine HCl 2.5% and tropicamide 1%). During scan acquisition, visualization of vitreous structures was prioritized by positioning the retina and choroid OCT signal posteriorly within the scan window. Vitreous imaging was performed on at least one eye of each participant, based on individual preference and ease of acquisition. Depending on subject cooperativity, one or both eyes were imaged. Scans with eye movement artifacts or excessively low signal-to-noise ratio without recognizable liquid vitreous spaces on individual B-scans precluding 3D reconstruction were excluded from the analysis.

Axial Length Measurements

Axial length was measured with the Zeiss IOL master 500 (Carl Zeiss Meditec, Inc).

Image Processing

Images were processed with ImageJ including the Fiji is just ImageJ (FIJI) image processing toolkit[12] version 1.53c with the plugin Trainable Weka Segmentation graphical user interface plugin (National Institutes of Health, Bethesda, MD, USA). A schematic of the segmentation pipeline is shown in Figure 1.

Image data were exported from the PlexElite device as IMG and imported into ImageJ using the Import>Raw command with parameters: 8-bit data, width: 1024 pixels, height: 1535 pixels, offset to first image: 0 bytes, number of images: 1024, gap between images: 0 bytes, white is zero: Yes, little-endian byte order: Yes. The imported OCT volume appeared horizontally and vertically inverted. The imported OCT volume was rectified by applying ImageJ's "Flip Vertically" command, then the "Flip Horizontally" command, to the entire stack. Although the image acquisition device obtained a nominal 12 mm cube scan, the captured OCT volume had greater axial resolution (1535 pixels), compared to the other dimensions (1024 × 1024 pixels), and the resultant voxels (3D pixels) had nonidentical dimensions. The voxels and the OCT volume were corrected to the nominal identical dimensions by using ImageJ's Scale command with the parameters x: 1.0, y: 0.666667, z: 1.0, width: 1024, height: 1024, depth: 1024, interpolation: bilinear average, creating a stack of 1024 B-scans, where each B-scan has dimensions 1024 × 1024 pixels. To improve the low signal-to-noise ratio, a running average of every 20 consecutive C-scans was performed using the

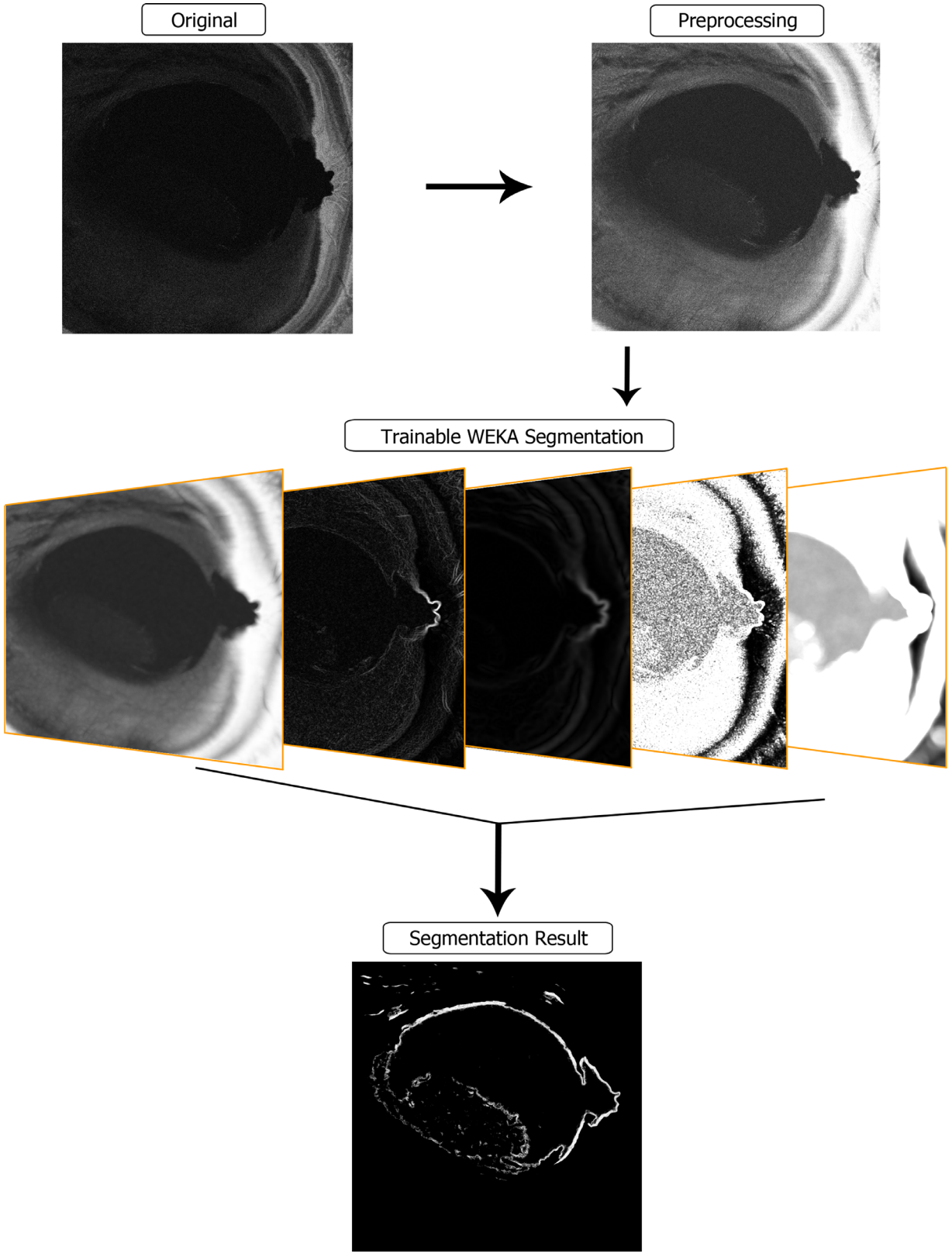

Figure 1. Segmentation pipeline. The original image is preprocessed to enhance contrast using the native PlexElite software. The resultant images are then subjected to Trainable Weka Segmentation, leading to an image with enhanced visualization of the interface between liquid and formed vitreous. A representative example of the training process is captured in Supplementary Video S1.

Running ZProjector plugin with the following parameters: running average size: 20, projection type: average intensity. The Running ZProjector plugin creates a new C-scan, in which each pixel consists of the average intensity of pixels in the same location in 20 sequential C-scans, repeated automatically in the anterior to posterior direction until fewer than 20 sequential C-scans remained (a script that automates this process is available as an online supplement). A new OCT volume was generated, containing the 1005 resulting C-scans. An enhanced vitreous viewing window was created for each OCT volume by using ImageJ's Brightness and Contrast control to adjust the dynamic range. Specifically, intensity values in the range $0, \bar{x}_V + \sigma_V$ were linearly rescaled to [0,255] while intensities larger than $\bar{x}_V + \sigma_V$ were set to 255. The value $\bar{x}_V$ is interpreted as the mean intensity of the entire OCT volume, and σ_V is interpreted as the standard deviation of the entire OCT volume. ImageJ's Histogram command (Analyze>Histogram>Include all Images) was used to find the OCT volume mean and standard deviation.

Trainable Weka Segmentation

Sobel filter and Variance filter for edge detection and Membrane Projections filter for 2D cross-sectional membrane detection from the Trainable Weka Segmentation toolkit were used to highlight the borders between the liquid spaces of the vitreous (the premacular bursa, prevascular vitreous fissures/cisterns, prepapillary gap) and more formed vitreous, as well as denser portions within the formed vitreous, which have been described in the context of vitreous degeneration.[13] The training stack was used for training the classifier. The C-scans in the training stack were examined, and a C-scan was chosen that depicted all of the following: the premacular bursa, the choroid, and the retina. The chosen C-scan was used as the basis of the initial algorithm training. The following settings for Trainable Weka Segmentation were applied: The "Sobel" filter, the "Variance" filter, and the "Membrane Projections" filter were selected. Membrane thickness was set to 5 pixels. Membrane patch size was set to 19 pixels. Minimum sigma was set to 1 pixel. Maximum sigma was set to 32 pixels.

The following classifier parameters were applied: the FastRandomForest classifier type was selected. "Batch Size" was set to "100." The "computeImportances" was set to "False." The "debug" was set to "False." The "doNotCheckCapabilities" was set to "False." The "maxDepth" was set to "0." The "numDecimalPlaces" was set to "0." The value for "numFeatures" was set to 4. This value was determined by using the "Save Feature Stack" button to generate a feature stack, then taking the square root of the number of images in the feature stack, and rounding to the nearest integer. The value for "numThreads" was set to 0 to autodetect based on CPU capability. The value for "numTrees" was set to 100. The value for the "seed" was automatically and randomly assigned by the software and was left unchanged.

After setting the classifier parameters, names were set for the two classes: "Septa" and "Other." Initial training of the classifier was conducted as follows. The ImageJ "Freehand" region of interest (ROI) selection tool with radius of 1 pixel was used to select pixels that did not represent a border between formed vitreous and a liquid vitreous space, by using the mouse to draw a line running roughly from one corner of the C-scan to the transverse opposite corner, with slight deviations from a straight-line path as needed to include a variety of areas of distinct quality, intensity, or pattern. For example, an effort was made to include areas of the extraocular spaces, the choroid, the retina, and the interfaces between anatomic regions, as well as more-dense or less-dense regions of non-membranous vitreous. The linear selection was continued in the same direction until it approached a membranous vitreous reflectivity and was stopped roughly 10 pixels away from the perceived membranous reflectivity. The selected line was labeled as class "Other" using the button in the user interface. A sample of pixels representing a border between formed vitreous and a liquid vitreous space was selected by using the ImageJ "Freehand" ROI selection tool with radius of 1 pixel to draw a line of 20 to 50 pixels in length, following the curvature of the membranous reflectivity. The selection was labeled as class "Septa" using the button in the user interface. Another freehand selection of radius 1 pixel was then started, approximately 10 pixels away from the other side of the membranous border, continuing towards the transverse opposite corner previously mentioned stopping if another membranous reflectivity is approached. Pixels were labeled in this alternating fashion until the transverse opposite corner was reached.

The "Train Classifier" button on the user interface was used to train the classifier with the labeled pixels. The resultant initial segmentation was adjusted and refined by examining the preview window for mis-classified regions, which were then corrected by making further linear ROI selections of 20 to 50 pixels in length, adding them to the appropriate class, and then using the "Train Classifier" button to interactively refine the classifier. Care was taken to use the fewest labels necessary to obtain a satisfactory segmentation. Once the first C-scan was satisfactorily segmented, the other C-scans in the stack were examined for

mis-classified areas, and corrected in the same manner. The classifier was saved, and the Training Stack was closed.

An example of the training process can be seen in online Supplementary Video S1.

A script was then used to apply the classifier to the Batch Processing Stacks in their respective directory. Once classification was complete, five hyperstacks with 2 channels each (one for each of the previously defined classes) were generated. The five hyperstacks were merged into one using FIJI's Concatenate tool. The channel arranger tool was used to remove the second channel, corresponding to class "Other", leaving only the channel corresponding to class "Septa". Thresholding was performed to remove the lower fifty percent of values. 24 blank C-scans were added to the anterior end of the stack. The original imported, rectified and scaled OCT volume was reconstructed in en-face orientation (the "Original En-face OCT Volume").

Image Display

TomViz (Tomviz for tomographic visualization of Nanoscale Materials, Version 1.8.0. Tomviz (2019) available at: https://tomviz.org/ (last accessed: January 2, 2020) was used to display tomography data from each stack as a maximum intensity projection. The algorithmically-enhanced vitreous OCT volume was displayed as a "Volume" visualization with the "Black, Blue and White" default false-color scheme included in TomViz. The retina and vasculature were overlaid as an additional "Volume" visualization by importing the unprocessed OCT volume, with the "Plasma" default false-color scheme included in TomViz.

Grading of Vitreous Degeneration

Eyes were graded for vitreous degeneration. Grade 1 was assigned to eyes with formed vitreous around the liquid spaces, and narrow prevascular vitreous fissures. Grade 2 was assigned to eyes with some heterogeneity of the vitreous outside of the liquid spaces and markedly enlarged prevascular vitreous fissures or fully formed cisterns. Grade 3 was assigned to eyes with marked vitreous degeneration characterized by heterogeneity and disorganization of the formed vitreous with tangled fibers and connection of liquid and degenerative spaces. Grades 1, 2, and 3 are illustrated in Figures 4A/4D, 4B/4E, and 4C/4F, respectively.

Statistical Analysis

Axial length and age data were tested for normal distribution using the Kolmogorov-Smirnoff test. Data are reported as averages and standard deviation. Data between groups were compared with an unpaired *t* test.

Results

Forty-seven eyes were imaged with the PlexElite. Key features of the vitreous, such as the premacular bursa, the prepapillary gap in the area of Martegiani and prevascular vitreous fissures and cisterns with various levels of vitreous degeneration could be visualized in the scans of all eyes imaged in this study. However, 13 eyes had to be excluded because of registration artifacts (n = 9) or excessively low signal-to-noise ratio (n = 4) precluding 3D reconstruction. Thirty-four eyes of 25 healthy subjects ranging in age from 7 to 34 years (mean 24.8 ± 6.85), and axial lengths between 23.2 and 26.0 mm (mean 24.7 ± 0.92; axial length was not obtained in five eyes) were included in this study.

Reconstruction of the vitreous anatomy using our machine- learning model reliably depicted the aforementioned features in three dimensions. The Sobel and variance filter for edge detection, as well as membrane projections filter for two-dimensional (2D) cross-sectional membrane detection from the Trainable Weka Segmentation toolkit reliably highlighted the borders between the liquid spaces of the vitreous and more formed vitreous (Fig. 1 and Supplementary Video S1). Representative 2D images of five of the 34 eyes are shown in Figures 2 to 4 (corresponding Supplementary Videos S2–S6 are available online). Figure 2 shows the right eye of a 38-year-old female with an axial length of 24.40 mm. The 3D reconstruction demonstrates the prepapillary gap in the area of Martegiani, which is separated from the premacular bursa by cortical vitreous, as is also evident on serial examination of the en face dataset (data not shown). The walls of narrow spaces overlying the large retinal blood vessels can be visualized. Figure 3 shows the right eye of a 34-year-old female with an axial length of 24.96 mm. The premacular bursa and area of Martegiani are present, but instead of the narrow fissures seen in Figure 2, ovoid spaces can be seen overlying the larger retinal vessels.

A range of vitreous degeneration could be observed on 3D reconstruction (Fig. 4). Although the liquid spaces were universally present in the 34 eyes, the vitreous surrounding them was variable in appearance. Thirteen of 34 eyes (38%) assigned vitreous degeneration grade 1 showed by definition a relatively uniform, solidly formed vitreous surrounding the liquid spaces, with slender perivascular vitreous fissures, examples of

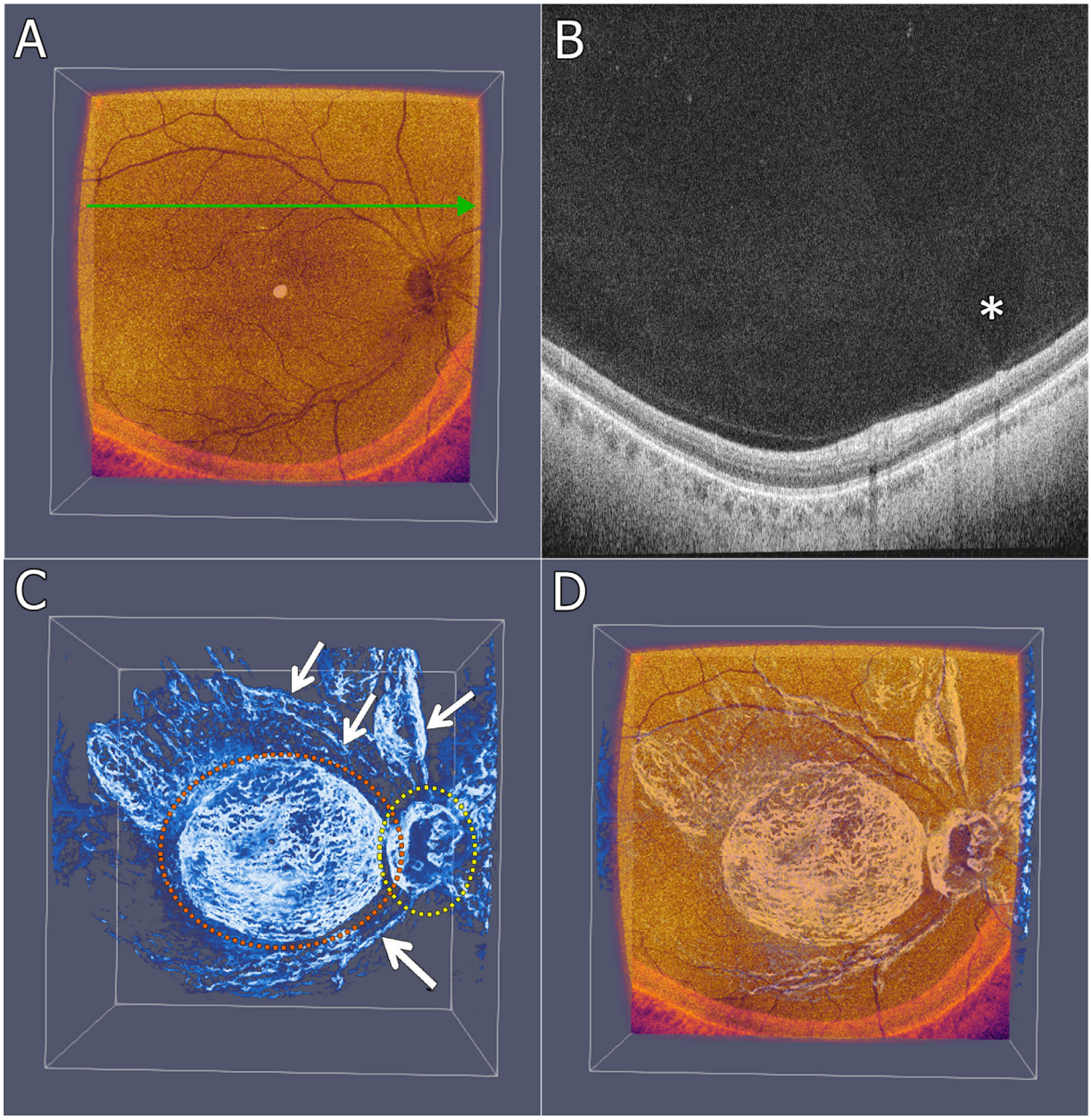

Figure 2. In this eye of a 38-year-old subject with an axial length of 24.4 mm, the posterior pole can be visualized in A, cross-sectional B-scan corresponding to the *green arrow* in A depicted in B highlighting a prevascular fissure that enlarges into a cistern (*asterisk*), the 3D reconstructed vitreous in C, and an overlay of the two in D. Clearly visible are the prepapillary gap (*yellow dotted oval*), the premacular bursa (*orange dotted oval*), and the prevascular vitreous fissures (*arrows*) overlying the large retinal vessels. The corresponding 3D movie of the 3D reconstruction can be viewed online in Supplementary Video S2.

which are depicted in Figures 2 and 4A and 4D. Grade 2 was defined by enlargement of the vitreous spaces with either enlarged perivascular vitreous fissures or fully formed cisterns, as in Figures 2 and 4B and 4E. The formed vitreous itself appeared more heterogeneous. This was present in 12 of 34 eyes. Advanced vitreous degeneration in grade 3 vitreous degeneration was defined as degenerative spaces surrounding the premacular bursa-prepapillary gap-complex, as well as connections between the various vitreous spaces (Figs. 4C, 4F). Furthermore, the vitreous surrounding these spaces was highly heterogeneous, with tangling of the vitreous fibers and a generally disorganized appearance of the 3D-reconstructed vitreous. This was present in nine of 34 eyes (26%). There was a trend toward more advanced vitreous degeneration with greater age (grade 1: 21 ± 7.4 years, grade 2: 24 ± 7.7 years, and grade 3: 27 ± 4.4 years) and axial length

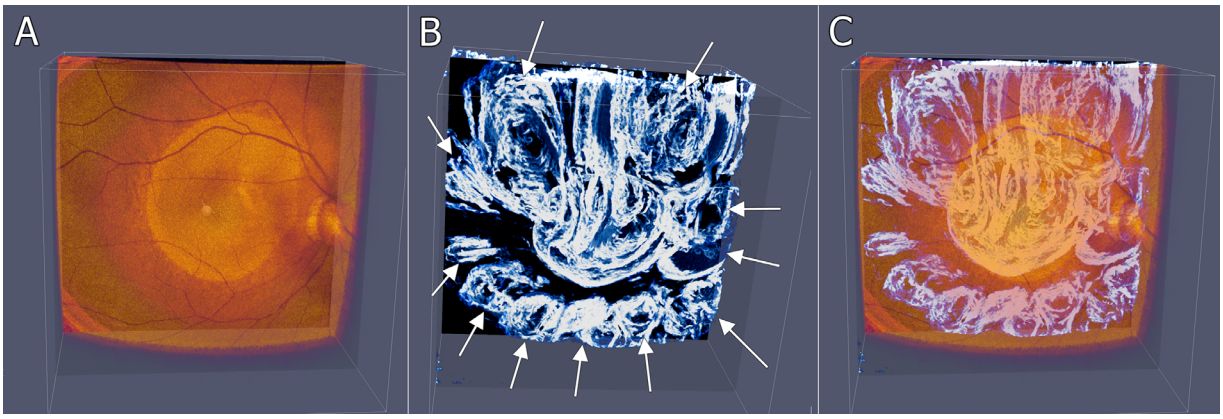

Figure 3. In this eye of a 34-year-old subject with and axial length of 26.0 mm, the retinal vasculature is again visualized in A, the 3D reconstructed vitreous in B, and an overlay of the two in C. The premacular bursa is surrounded by a petalliform circle of cisterns (*white arrows*). The corresponding movie of the 3D reconstruction can be viewed online as Supplementary Video S3.

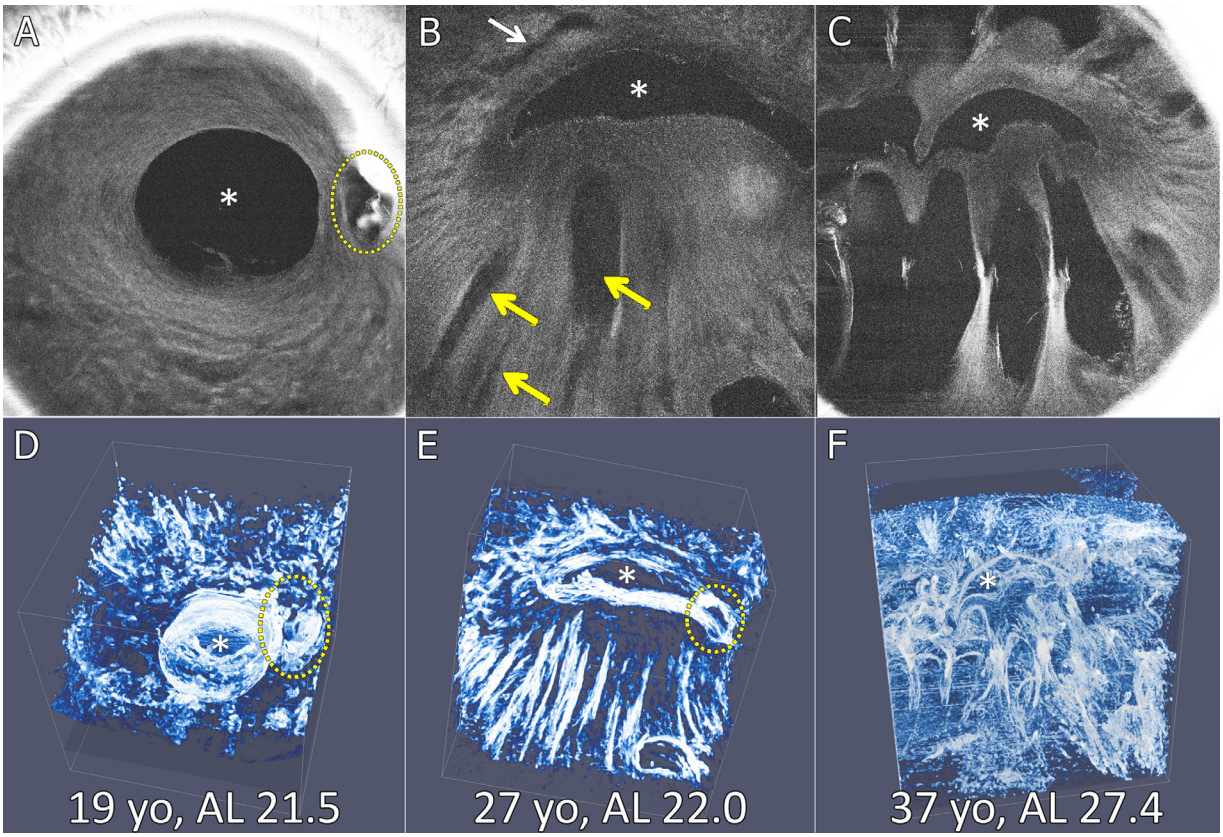

Figure 4. A spectrum of vitreous degeneration was apparent in the studied population. A, B, and C are *en face* scans, D, E, and F are the corresponding 3D reconstructions of the posterior vitreous from different eyes (corresponding 3D movies can be viewed online as Supplementary Videos S4, S5, and S6, respectively). A and D were acquired in the right eye of a 19-year-old subject with an axial length of 21.5 mm. A round premacular bursa (*asterisk*), and relatively uniform surrounding vitreous are seen in the en face scan in A. The prepapillary gap in the area of Martegiani (*yellow dotted oval*) is separated from the premacular bursa by formed vitreous. B and E were acquired in the right eye of a 27-year-old individual with an axial length of 22.0 mm. The premacular bursa (*asterisk*) has assumed a horizontally elongated shape on the en face scan in B and is found to connect with the prepapillary gap on serial examination of the en face dataset. The vitreous is more heterogeneous, compared to A and D, with several slender liquid spaces, one following the superior arcade (*white arrow*), and several larger spaces in a vertical direction inferiorly (*yellow arrows*). The 3D reconstructions highlight the superior direction of the premacular bursa-prepapillary gap-complex, as well as the heterogeneity of degenerating vitreous. C and F were acquired in the left eye of a highly myopic 37-year-old subject with an axial length of 27.4 mm. Advanced vitreous degeneration can be appreciated in the en face image in C, with liquid spaces surrounding the premacular bursa-prepapillary gap-complex (*asterisk*) that surpass the latter in size. The formed vitreous surrounding these spaces is highly heterogeneous, with tangling of the fiber network, leading to the disorganized appearance of the 3D-reconstructed vitreous in F.

(grade 1: 23.1 ± 2.10 mm, grade 2: 23.8 ± 0.98 mm and grade 3: 25.3 ± 1.55mm). However, only the axial length difference between groups 1 and 3 approached statistical significance with a P value = 0.051.

Discussion

Because the vitreous is mostly transparent, details of its anatomy are difficult to study in vivo. Postmortem studies are complicated by the delicacy of vitreous structure, and susceptibility to decay. Worst identified the premacular bursa in 1977[1] in cadaveric eye preparations, with further refinements made by Jongebloed and Worst in 1987[2] and subsequently Kishi and Shimizu in 1990.[3] Kishi and Shimizu[3] gave this structure the name "posterior precortical vitreous pocket" to highlight the presence of cortical vitreous fibers at the bursa-retina interface. Eisner[4,5] described hyporeflective, liquid vitreous structures overlying the retinal blood vessels of cadaveric eyes and named them "prevascular fissures." We described the presence of prevascular spaces first on cross-sectional OCT,[12] and later confirmed them to indeed follow the course of the retinal blood vessels with en face analysis of SS-OCT cube scans.[9] A few years later, Jongebloed and Worst[2] described a system of "hollow" spaces they termed "cisterns." Sebag[6] described a spectrum of vitreous degeneration in darkfield microscopy preparations of cadaver eyes. We described varying degrees of vitreous degeneration on cross-sectional[13] and en face OCT analysis[9] and found the width of the prevascular fissures to be correlated with vitreous degeneration,[13] raising the possibility of the fissures being precursors to the cisterns described by Jongebloed and Worst.[2]

OCT imaging has permitted the in vivo examination of the vitreous and not only confirmed the presence of structures previously reported in cadaver eyes, but also allowed to better characterize their relationships to each other, as well as their role in the pathogenesis of important retinal diseases. In a recent study, we optimized en face SS-OCT to visualize the vitreous structure.[9] In the present study, we used machine learning to reconstruct these image stacks into 3D visualizations of the vitreous. The Plex-Elite software already performs signal enhancement through image averaging and other methods. However, the signal from the vitreous remains too weak to allow visualization of the 3D anatomy of its gel and liquid portions without further post-processing.

Weka[11] provides machine-learning algorithms and other tools for data analysis. The Trainable Weka Segmentation plugin for ImageJ implements the Random Forest classifier from the Weka toolkit with a graphical interface for classifying pixels within images. Using this machine-learning algorithm, we were able to demonstrate key features of the vitreous anatomy, such as the premacular bursa, prepapillary gap in the area of Martegiani, prevascular fissures and cisterns as well as a spectrum of vitreous degeneration. Not only were these findings consistent with findings from previous work performed with different OCT machines by various groups but also expanded into 3D and allow for a more complete appreciation of the vitreous anatomy over the posterior pole.

Our findings concur with both postmortem and in vivo findings by several other researchers. The en face scans depicted in our previous work[9] and Figure 4 bear a striking resemblance with Eisner's slit-lamp photographs of fresh cadaveric vitreous,[5] an example of which is reproduced in Figure 5A. The 3D reconstruction of these spaces from this dataset, which could previously only be reassembled in one's mind after scrolling through multiple individual OCT slices, shows a configuration of liquid spaces in the vitreous cavity that was first demonstrated by Worst[1] in ink-injected cadaver eyes (Fig. 5B) and is now routinely appreciated by the vitreoretinal surgeon during triamcinolone-assisted vitrectomy (Fig. 5C), where the steroid particles highlight the walls of the premacular bursa, cisterns, and the prepapillary gap and give rise to an appearance quite similar to the ones seen in our 3D reconstructions (Fig. 3B/C).[14] The clinician routinely appreciates a wide spectrum of vitreous synchesis and syneresis on clinical examination, and the vitreoretinal surgeon encounters this during vitrectomy. We first described and graded vitreous degeneration on cross-sectional OCT.[13] Specifically, formation of degenerative fissure planes, enlargement of the liquid spaces of the vitreous, followed by connections between the first and the latter, as well as with each other could be observed. However, cross-sectional analysis can only hint at the appearance of the degenerating vitreous in three dimensions. En face SS-OCT scans and their 3D reconstruction highlight a wide spectrum of vitreous degeneration in vivo,[9] as illustrated in Figure 4. Kishi and Shimizu[3] pointed out analogous findings in cross-sectional photos of postmortem preparations (Fig. 5D). Sebag[6] made similar observations in fresh, unfixed cadaveric human vitreous preparations examined with dark-field slit-microscopy and was able to visualize vitreous with relatively formed solid vitreous (Fig. 5E) quite similar to our findings illustrated in a representative eye in Figures 4A and 4D or degenerated syneretic vitreous characterized by tangled fibers (Fig. 5F), an image that bears a striking resemblance with the 3D reconstruction shown in Figure 4F. Although it has been demonstrated that vitreous degeneration correlates with increasing age and axial length, only a trend was found in this

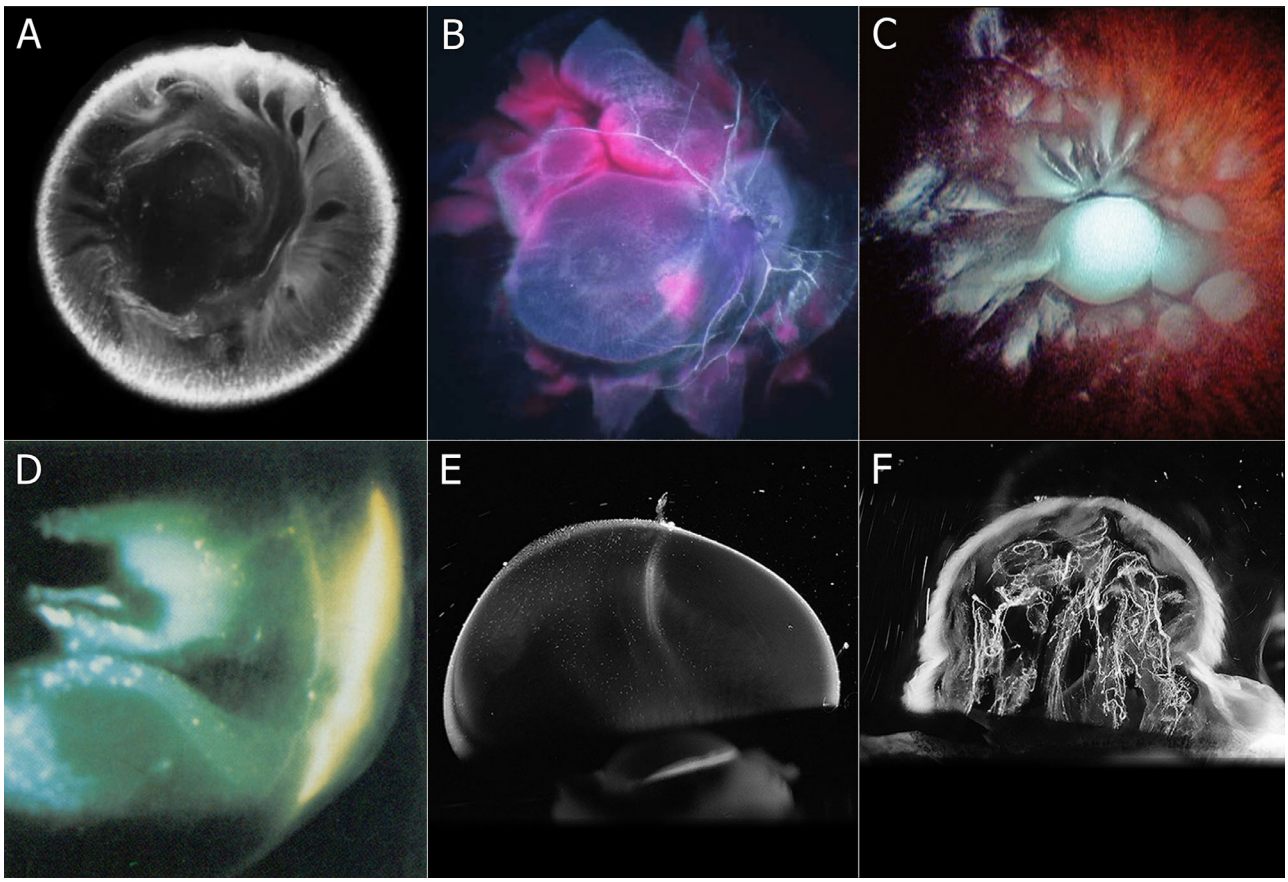

Figure 5. En face SS-OCT and machine learning assisted 3D reconstruction concur with in-vivo and post-mortem findings of the vitreous anatomy. (A) Slit-lamp photography of cadaveric human vitreous (Eisner[5]), depicts the premacular bursa and prevascular cisterns in a similar cross-sectional fashion as what can be seen in the en face images of the OCT dataset which are the basis of the 3D reconstruction. Rather than in cross-section, (B) ink-injected cadaveric vitreous (image courtesy of J. Worst) and (C) triamcinolone-stained posterior cortical vitreous during vitrectomy (Fine and Spaide[11]) show the liquid spaces of the vitreous as they appear in our 3D reconstruction (compare to Fig. 3). Various degrees of vitreous degeneration have been described in (D) fluorescein-stained cadaveric vitreous (Kishi[3]), and dark-field photographs of cadaveric vitreous of (E) a young eye with little and (F) an older eye with pronounced vitreous degeneration (Sebag[6]), quite similar to what we observed in our study population (compare to Fig. 4).

study,[13] possibly because of the smaller sample size. Furthermore, vitreous degeneration is interindividually variable, and this was evident in this study, where a seven-year-old showed grade 2 degeneration, and a 33-year-old showed grade 1 degeneration.

Shortcomings of this methodology include its dependence on excellent scan quality, which is limited by subject cooperativity (fixation loss or head movement, blinking, and tear film abnormalities), media clarity, and OCT acquisition speed and quality. Thirteen of 47 (28%) scans in our study had to be excluded because of linear artifacts from poor scan registration and excessively low signal-to-noise ratio for the purpose of this study. Because of significant variability in dynamic ranges of the input data, human training of the machine learner was necessary for all images. It may be possible to overcome this limitation through improvements in intensity normalization algorithms in the future. Processing times for the 1024-pixel cube volumes were directly correlated with the number of pixels labeled during training of the classifier and ranged from 30 minutes to two hours, using a multithreaded process on a system with a 32-core AMD Ryzen Threadripper 3970x and 64GB of RAM, which limits the clinical utility of this method. However, it may be possible to reduce the time requirement to three to 15 minutes (an eight-times reduction) by applying this method to lower-resolution 512-pixel cube volumes. Additionally, future implementation of GPU-acceleration may greatly decrease the processing time by a yet indeterminate amount.

Furthermore, image depth and width are limited, so that currently only a relatively small volume of the posterior pole beyond the vascular arcades and optic nerve in the posterior vitreous can be visualized. With rapid development of OCT technology, it can be hoped that these hurdles will be overcome in the future.

To the best of our knowledge, this is the first translational report of a methodology that allows 3D representation of the vitreous anatomy in a fashion that concurs with various intraoperative and postmortem studies in that it depicts the liquid vitreous spaces in relation to the retinal surface, as well as clinically important features of vitreous degeneration such as enlarged liquid spaces and their connections, as well as tangling of the vitreous fiber network. It has the promise of defining the role the vitreous plays beyond the vitreoretinal interface in several common and important conditions, where this has been illustrated on cross-sectional B-scan analysis, such as in the vitreomacular traction–macular hole spectrum of diseases[15] or proliferative diabetic retinopathy.[16]

Acknowledgments

Supported by the Macula Foundation, Inc.

Disclosure: **M. Engelbert,** Genentech (C); **K.B. Freund,** Allergan (C), Bayer (C), Genentech (C), Heidelberg Engineering (C), Novartis (C), Regeneron (C), Zeiss (C), Genentech/Roche (R); **A. Thi,** None

References

1. Worst JG. Cisternal systems of the fully developed vitreous body in the young adult. *Trans Ophthalmol Soc UK*. 1977;97:550–554.
2. Jongebloed WL, Worst JFG. The cisternal anatomy of the vitreous body. *Doc Ophthalmol*. 1987;67(1–2):183–196.
3. Kishi S, Shimizu K. Posterior Precortical Vitreous Pocket. *Curr Eye Res*. 1990;108:979–982.
4. Eisner G. *Biomicroscopy of the Peripheral Fundus*. New York: Springer-Verlag; 1979.
5. Eisner G. Clinical anatomy of the vitreous. In: Jacobiec F, ed. *Ocular Anatomy, Embryology, and Teratology*. Philadelphia: Harper & Row Publishers; 1982:391–424.
6. Sebag J. *Vitreous – in Health & Disease*. New York: Springer; 2014:viii.
7. Itakura H, Kishi S, Li D, Akiyama H. Observation of posterior precortical vitreous pocket using swept-source optical coherence tomography. *Invest Ophthalmol Vis Sci*. 2013;54:3102–3107.
8. Schaal KB, Pang CE, Pozzoni MC, Engelbert M. The premacular bursa's shape revealed in vivo by swept-source optical coherence tomography. *Ophthalmology*. 2014;121:1020–1028.
9. Leong BCS, Fragiotta S, Kaden TR, Freund KB, Zweifel S, Engelbert M. OCT en face analysis of the posterior vitreous reveals topographic relationships among premacular bursa, prevascular fissures, and cisterns. *Ophthalmol Retina*. 2020;4:84–89.
10. Arganda-Carreras I, Kaynig V, Rueden C, et al. Trainable Weka segmentation: a machine learning tool for microscopy pixel classification. *Bioinformatics*. 2017;33:2424–2426.
11. Hall M, Frank E, Holmes G, Pfahringer B, Reutemann P, Witten IH. The Weka data mining software: an update. *ACM SIGKDD Eplor Newslett*. 2009;11:10–18.
12. Schindelin J, Arganda-Carreras I, Frise E, et al. Fiji: an open-source platform for biological-image analysis. *Nat Methods*. 2012;9:676–682.
13. Pang CE, Schaal KB, Engelbert M. Association of prevascular vitreous fissures and cisterns with vitreous degeneration as assessed by swept-source optical coherence technology. *Retina*. 2015;35:1875–1882.
14. Fine HF, Spaide FR. Visualization of the posterior precortical vitreous pocket in vivo with triamcinolone. *Arch Ophthalmol*. 2006;124:1663.
15. Ghadiali Q, Zahid S, Dolz-Marco R, Tan A, Engelbert M. An assessment of vitreous degeneration in eyes with vitreomacular traction and macular holes. *J Ophthalmol*. 2017;2017:6834692.
16. Vaz-Pereira S, Dansingani KK, Chen KC, Cooney MJ, Klancnik JM, Jr, Engelbert M. Tomographic relationships between retinal neovascularization and the posterior vitreous in proliferative diabetic retinopathy. *Retina*. 2016;37:1287–1296.

Supplementary Material

Supplementary Video 1. Example of the training process using Trainable Weka Segmentation.

Supplementary Video 2. 3D-reconstruction of the vitreous in a 38-year-old subject with axial length 24.4 mm.

Supplementary Video 3. 3D-reconstruction of the vitreous in a seven-year-old subject.

Supplementary Video 4. 3D-reconstruction of the vitreous in a 19-year-old subject with axial length 21.5 mm.

Supplementary Video 5. 3D-reconstruction of the vitreous in a 27-year-old subject with axial length 22.0 mm.

Supplementary Video 6. 3D-reconstruction of the vitreous in a 37-year-old subject with axial length 27.4 mm.